

Ultrafast photoionization dynamics at high laser intensities in the xuv regimeB. Kaiser,^{*} A. Vagov, and V. M. Axt*Institut für Theoretische Physik III, Universität Bayreuth, D-95440 Bayreuth, Germany*

U. Pietsch

Institut für Festkörperphysik, Universität Siegen, D-57068 Siegen, Germany

(Received 27 June 2011; published 28 October 2011)

We study the ionization dynamics in the soft-x-ray regime for high intensities and short pulses for excitations near the ionization threshold. Using a one-dimensional helium atom model, we compare exact numerical solutions with time-dependent Hartree-Fock results in order to identify the role of electron-electron correlations. At moderate intensities but still in the x-ray and short-pulse regime, we find that the Hartree-Fock theory reproduces well the dynamics of the ground-state occupation, while at high intensities strong correlation effects occur for excitations close to the threshold. From their characteristic momentum distributions, we can identify contributions to the double ionization from sequential three-photon and nonsequential or sequential two-photon processes. At elevated intensities these contributions deviate from their usual intensity scaling due to saturation effects, even though the total double-ionization probability stays below 10%. Furthermore, analysis of the time evolution of the momentum distribution reveals signatures of the energy-time uncertainty which indicate a coherent regime of the dynamics.

DOI: [10.1103/PhysRevA.84.043431](https://doi.org/10.1103/PhysRevA.84.043431)

PACS number(s): 32.80.Fb, 42.65.Re, 32.80.Aa

I. INTRODUCTION

The availability of a new generation of free-electron-laser (FEL) sources, which deliver highly intensive radiation in the extreme ultraviolet (xuv) or x-ray regime enables studies of light-matter interaction under so-far-inaccessible extreme conditions and allows for new kinds of experiments including the recording of single-shot x-ray diffraction patterns [1,2] and the structure analysis of nonperiodic structures [3]. Decisive for the success of such experiments is also the realization of ultrashort pulses which test the sample on a time scale before the damage process has significantly progressed [4]. However, short and intense pulses imply a fast electron dynamics comparable with the pulse length. In particular, ionization processes take place on short time scales, and it is expected that the corresponding changes of the electronic structure will have a noticeable effect on the measured diffraction patterns [5]. Thus, a detailed knowledge of the dynamics of ionization processes is of central importance for the interpretation and/or development of experiments with new physics using the current FEL sources.

The theoretical description of ionization processes is a great challenge for theory, in particular when correlations cannot be ignored, as, e.g., for the nonsequential two-photon double ionization of helium under xuv and vacuum ultraviolet (vuv) conditions [6–12]. Correlated two-photon-ionization processes are commonly found also for other systems such as, e.g., neon [13–15]. For atoms with more electrons, the situation is even more complex, and correlations in the form of a collective electron motion have been discussed as a possible explanation for the observed highly charged xenon ions (up to Xe^{21+}) [16]. However, the direct solution of the Schrödinger equation is impossible for larger systems, unlike helium. Mostly, ionization processes for atoms with many electrons

are described by rate equations [17,18] and, depending on the excitation conditions, often a good agreement with experiments is achieved. In addition, currently several approximate many-particle approaches, including Green's function methods [19], the time-dependent Hartree-Fock approach [20], multiconfigurational Hartree-Fock theories [21,22], and time-dependent density-functional theory [23], are being adapted to the ionization problem. It is therefore of great importance to identify conditions under which approximate methods give qualitatively correct results and what types of deviations have to be expected when correlations dominate that are disregarded in such theories.

Furthermore, reaching the regime of high intensities and ultrashort pulses [24] raises many specific questions. Here, a full account of the nonlinear dynamics beyond leading-order perturbation theory is required that captures, e.g., saturation effects [25], multiple multiphoton ionization [16,26,27], and other nonlinearities in the ionization process that may also affect the secondary emission seen in diffraction measurements. Also, the use of ultrashort pulses introduces new perspectives. Recent calculations reveal that, even for photon energies that are supposed to be in the purely sequential regime, the two electrons emitted in a double-ionization process exhibit features that qualitatively deviate from the standard behavior in this regime [28,29]. In particular, a predominantly symmetric energy sharing for decreasing pulse duration is predicted, and the electrons are preferentially emitted in opposite directions [28]. Moreover, currently it is unclear how short the pulse durations have to be for a regime of coherent dynamics to be encountered where quantum superposition states are important and signatures of the energy-time uncertainty become noticeable. While often one process can be identified that dominates the ionization dynamics for given excitation conditions, when a system is driven with ultrashort pulses competition and quantum interference between different pathways, e.g., direct ionization and Auger-type ionization [30,31], are also conceivable.

^{*}benjamin.kaiser@uni-bayreuth.de

A main focus of this paper is to explore theoretically the role of correlations due to the electron-electron interaction in the ionization dynamics for highly intense near-threshold radiation. To this end it is advantageous to consider a model where these correlations can be fully taken into account. A simple model system that can be treated completely is the one-dimensional (1D) helium atom; this model has been applied extensively to ionization phenomena in the optical and infrared regimes [32,33]. Although quantitatively such models cannot be expected to match full three-dimensional (3D) calculations in all respects, for many qualitative aspects physically meaningful results can be anticipated as 1D model atoms are known to share many properties with real atoms [34,35]. Here, we solve numerically the Schrödinger equation for the 1D helium model for intensities up to $\approx 10^{16}$ W/cm² and short pulses in the femtosecond regime near the thresholds for single-photon single-electron ionization and two-photon double ionization of helium. We compare these calculations with results of the time-dependent Hartree Fock theory (TDHF) which accounts for the electron-electron interaction on the mean-field level but describes the system at all times by a single Slater determinant and thus neglects genuine many-particle correlations. The comparison of numerical complete results with TDHF calculations allows us to evaluate the importance of genuine correlations under high-intensity, soft-x-ray, and short-pulse excitation conditions. From this comparison, we find that the impact of interaction-induced correlations is particularly strong in close vicinity to the ionization thresholds and even affects signals that are dominated by single-ionization processes.

Another goal of the present paper is to separate different types of double-ionization processes and to follow their respective dynamics. To this end we discuss the momentum distributions of the two emitted electrons. We analyze the competition between sequential three-photon and sequential and nonsequential two-photon double-ionization processes. Our results reveal a noticeable influence of the energy-time uncertainty during the pulse. A separate analysis of the time evolution of different processes confirms that different contributions to the double ionization take place on roughly the same time scale that is completed after the pulse is gone. From the time traces we also find indications that electrons which are emitted in the same direction can be recaptured after they have first traveled more than five atomic Bohr radii away from the core.

II. MODEL

The basis for our present work is the 1D helium model described by the Hamiltonian

$$H = \sum_{j=1,2} \frac{1}{2m} [p_j + eA(t)]^2 + \sum_{j=1,2} V_c(x_j) + V_e(|x_1 - x_2|), \quad (1)$$

where $V_c(x)$ is the core potential and $V_e(|x_1 - x_2|)$ is the electron-electron interaction. Due to the restriction to one dimension, it is necessary to choose a regularized core potential $V_c(x)$ without singularity. Here, we shall use $V_c(x) = -\frac{U_0}{\cosh^2(x)}$ which leads to $V_e(|x_1 - x_2|) = \frac{U_0}{N \cosh^2(x)}$ with $N = 2$. If U_0 is

set to 3.0 atomic energy units, our model yields a ground-state energy ($E_0 = -81$ eV) and ionization thresholds (single ionization $I_p^{(1)} = 27$ eV, double ionization $I_p^{(2)} = 54$ eV) comparable to those of the 3D helium model [6,8]. The single dimension retained in the model can be identified with the polarization axis of a linearly polarized radiation field, as in this direction the strongest field-induced dynamics is expected [6]. The corresponding component of the electrical field $\mathcal{E}(t)$ is related to the vector potential component in the polarization direction, $A(t)$, by $\mathcal{E} = -\dot{A}$. The field is represented as

$$\mathcal{E}(t) = \mathcal{E}_0 \cos[\omega(t - t_0)] \exp\left(-\frac{(t - t_0)^2}{2t_p^2}\right). \quad (2)$$

We assume that the system is initially in the ground state and choose the center of the pulse as the origin of time, i.e., we set $t_0 = 0$. The pulse duration is controlled by the parameter t_p . Current FEL sources typically can operate at pulse lengths down to about 10 fs [36,37]. Recent measurements with the Linac Coherent Light Source at Stanford have reached pulse durations in the few-femtosecond region [24,36], thus making the ultrafast dynamics that is the focus of the present paper experimentally accessible. For the present study we adjust t_p in such a way that the full width at half maximum of the field amplitude is 1.6 fs. Exact results for the field-driven dynamics in this model are easily obtained by direct numerical solution of the corresponding Schrödinger equation for the two-electron wave function, which is a spin singlet when the dynamics starts in the electronic ground state. Here, we have solved the time-dependent Schrödinger equation in k -space representation. The direct numerical solution of the Schrödinger equation for systems with more than two particles is currently out of reach for 3D systems and is also rather demanding in the 1D limit. Therefore, approximate approaches like the TDHF theory [20] are needed for larger systems, and it is important to know under which circumstances these methods are reliable. The treatment of ionization problems within the TDHF framework has a long tradition [20,38,39]. The TDHF theory has been found to give reasonable excitation and ionization cross sections under various excitation conditions [20,39]. However, one should be aware of intrinsic restrictions of the TDHF theory that apply particularly to ionization processes in small systems like helium. An often discussed restriction comes from the fact that, when a two-electron system in a singlet state is represented as a single Slater determinant, then both electrons must occupy the same single-particle state [22,40], i.e., the spatial part of the wave function is a symmetric product, $\psi(r_1, r_2, t) = \varphi(r_1, t)\varphi(r_2, t)$. Expanding $\varphi(r, t)$ in a complete set of single-particle orbits, it is seen that the function $\psi(r_1, r_2, t)$, like the fully correlated wave function, provides probabilities for single and double ionization as well as for leaving the system unionized, but the factorized form of $\psi(r_1, r_2, t)$ imposes relations between the corresponding coefficients which will in general not hold for the fully correlated solution [20]. Whether or not these restrictions are severe strongly depends on excitation conditions and the considered signal. For example, for an excitation at wavelength $\lambda = 780$ nm the double-ionization yields of helium calculated within the TDHF theory deviate strongly from the results of the full solution of the Schrödinger equation, while

single-ionization yields are nicely reproduced [32]. At $\lambda = 248$ nm the TDHF calculation also gives a reasonable account of double-ionization yields [32]. To the best of our knowledge, the validity of the TDHF method has not been systematically tested for the high frequencies and intensities in the short-pulse regime that are considered in the present paper.

TDHF results are most easily obtained by following the time evolution of the reduced density matrix, which is defined by the expectation value $\langle c_{k_1\sigma_2}^\dagger c_{k_2\sigma_2} \rangle$, where $c_{k\sigma}^\dagger$ and $c_{k\sigma}$ create or annihilate an electron with wave number k and spin σ . Setting up Heisenberg equations of motion for these operators using the Hamiltonian Eq. (1) in second quantization results in an infinite hierarchy of equations of motion for expectation values involving an increasing number of operators $c_{k\sigma}^\dagger$ or $c_{k\sigma}$. The TDHF theory assumes that the system state can be approximated at any time by a single Slater determinant. This assumption leads to a closed set of equations of motion as all higher-order expectation values factorize. In this way we obtain

$$\begin{aligned}
 i\hbar \frac{d}{dt} \langle c_{k_1\sigma_1}^\dagger c_{k_2\sigma_2} \rangle &= \left(\frac{\hbar^2}{2m} (k_2^2 - k_1^2) + \frac{e}{m} A(t) \hbar (k_2 - k_1) \right) \langle c_{k_1\sigma_1}^\dagger c_{k_2\sigma_2} \rangle \\
 &- \sum_q \tilde{V}_c(q) [\langle c_{k_1+q\sigma_1}^\dagger c_{k_2\sigma_2} \rangle - \langle c_{k_1\sigma_1}^\dagger c_{k_2+q\sigma_2} \rangle] \\
 &+ \sum_{\substack{k',q \\ \sigma'}} \tilde{V}_e(q) [\langle c_{k_1\sigma_1}^\dagger c_{q+k_2\sigma_2} \rangle \langle c_{k'\sigma'}^\dagger c_{-q+k'\sigma'} \rangle \\
 &- \langle c_{k_1\sigma_1}^\dagger c_{-q+k'\sigma'} \rangle \langle c_{k'\sigma'}^\dagger c_{q+k_2\sigma_2} \rangle] \\
 &- \sum_{\substack{k',q \\ \sigma'}} \tilde{V}_e(q) [\langle c_{q+k_1\sigma_1}^\dagger c_{k_2\sigma_2} \rangle \langle c_{-q+k'\sigma'}^\dagger c_{k'\sigma'} \rangle \\
 &- \langle c_{q+k_1\sigma_1}^\dagger c_{k'\sigma'} \rangle \langle c_{-q+k'\sigma'}^\dagger c_{k_2\sigma_2} \rangle], \quad (3)
 \end{aligned}$$

where $\tilde{V}_c(q)$ and $\tilde{V}_e(q)$ are the Fourier transforms of the core potential $V_c(x)$ and the electron-electron interaction $V_e(x)$, respectively. The initial values of $\langle c_{k_1\sigma_1}^\dagger c_{k_2\sigma_2} \rangle$ are determined from a static self-consistent calculation of the Hartree-Fock ground state, which yields a stationary solution of Eq. (3). The time evolution of $\langle c_{k_1\sigma_1}^\dagger c_{k_2\sigma_2} \rangle$ is then obtained by iterating Eq. (3) in time.

III. DYNAMICS OF THE GROUND STATE

An important quantity of interest is the occupation probability of the ground state P_0 as it reflects the total ionization yield. Furthermore, it has a strong influence on x-ray scattering patterns. P_0 can easily be extracted from the wave function or the reduced density matrix by projecting on the ground state.

In Fig. 1 we have plotted the limiting value of P_0 for long times after the interaction with the radiation as a function of photon energy for two excitation intensities $I_1 = 3.5 \times 10^{14}$ W/cm² and $I_2 = 5.6 \times 10^{13}$ W/cm². We compare the numerically exact solution with the results of TDHF theory. The threshold for one-photon single ionization is in both cases at $\hbar\omega \approx 27$ eV, which results in a sharp decrease of the ground-state occupation for higher photon energies.

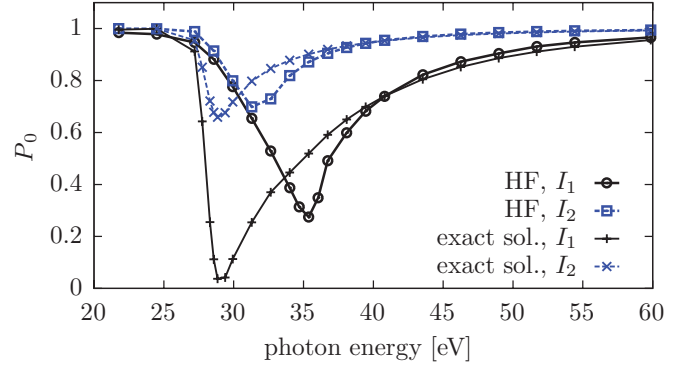


FIG. 1. (Color online) Occupation probability of the ground state P_0 as a function of the photon energy for the two intensities $I_1 = 3.5 \times 10^{14}$ W/cm² and $I_2 = 5.6 \times 10^{13}$ W/cm².

Below this threshold we observe a weak ionization which results from multiphoton processes. All four curves exhibit a sharp minimum above the threshold, and as expected the total ionization decreases when the intensity is reduced. In the Hartree-Fock approximation the minimum is less pronounced and shifts to higher energies with rising intensity, while in the exact calculation its position is almost independent of the intensity. The two calculations become more similar the lower the intensity. For photon energies above 40 eV the Hartree-Fock curves essentially coincide with the exact results. In order to understand the origin of the differences between Hartree-Fock and Schrödinger equation calculations, it is instructive to look at the time evolution of P_0 , which is shown in Fig. 2 for the higher intensity from Fig. 1 and for two photon energies.

Let us first concentrate on the results for an excitation at $\hbar\omega = 38$ eV [Fig. 2(a)] which for both levels of the theory is above the minimum in the ground-state occupation. Here, the Hartree-Fock result agrees qualitatively well with the full

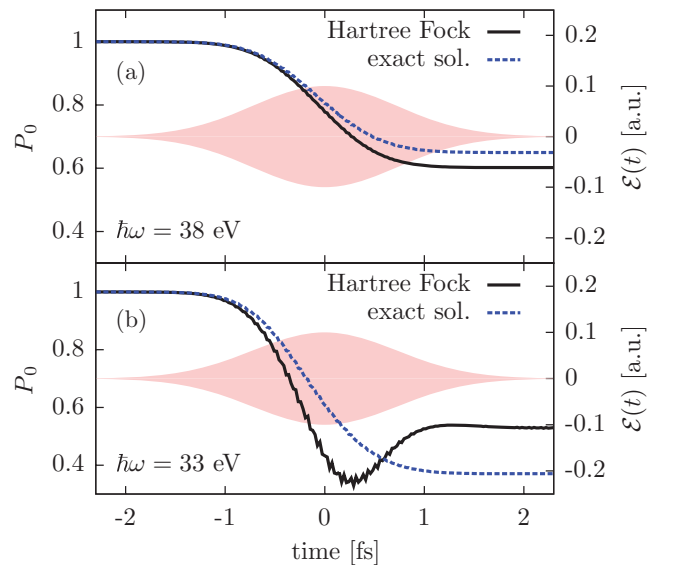


FIG. 2. (Color online) Time evolution of the ground-state occupation P_0 for excitations with an intensity $I_1 = 3.5 \times 10^{14}$ W/cm² and two photon energies: (a) $\hbar\omega = 38$ eV and (b) $\hbar\omega = 33$ eV. The red filled area represents the envelope of the electrical field \mathcal{E} .

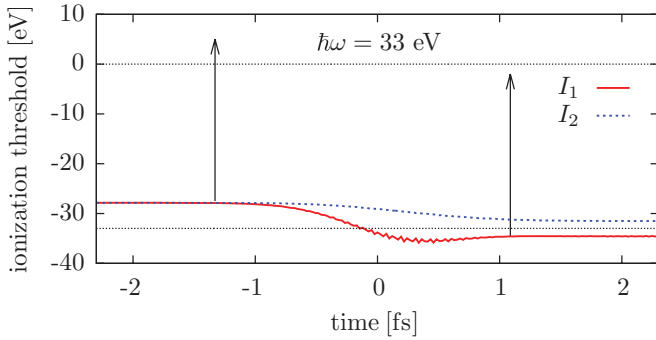


FIG. 3. (Color online) Time dependence of the lowest Hartree-Fock eigenvalues obtained by diagonalizing the mean-field Hamiltonian at each time step for the two intensities $I_1 = 3.5 \times 10^{14}$ W/cm² and $I_2 = 5.6 \times 10^{13}$ W/cm². The arrow represents the energy of a single photon, $\hbar\omega = 33$ eV.

calculation. The occupation probability of the ground state decreases monotonically during the laser pulse and after the pulse stays at a value of about $\sim 60\%$.

In contrast, a nonmonotonic time evolution of P_0 is found in the Hartree-Fock calculation for an excitation closely above the single-ionization threshold [Fig. 2(b)]. In comparison to the exact solution, the atom is ionized faster in the Hartree-Fock calculation until the ground state is populated with only $\sim 34\%$ probability. Then the ionization stops and a recombination is observed even though the pulse is still driving the system. In order to understand this feature of the Hartree-Fock approach we have diagonalized the Hartree-Fock Hamiltonian at each time step. Note that the Hartree-Fock solution is in our case equivalent to a mean-field treatment of the Hamiltonian Eq. (1), and thus the Hartree-Fock Hamiltonian depends parametrically on the time-dependent values of the reduced density matrix. Consequently, the energy eigenvalues obtained by the diagonalization depend on time. These values effectively determine the ionization threshold. Figure 3 shows the time evolution of the lowest eigenvalue for an excitation energy of $\hbar\omega = 33$ eV for the two intensities from Fig. 1. With ongoing ionization the lowest eigenvalue decreases because the screening of the core potential by the mean field of the electrons is reduced and thus the binding of the remaining charges is enhanced. At higher intensity the binding energy is larger than the photon energy. Once it lies sufficiently above this energy, single-photon processes are significantly suppressed and the ionization stops even though the pulse is still driving the system. From this time on the pulse generates only transient virtual excitations which disappear after the pulse. This is seen as the recovery of the ground-state occupation in Fig. 2(b).

For high enough photon energies, this stopping of the ionization does not take place as the binding is never larger than the photon energy. This is the case in Fig. 2(a) where also the Hartree-Fock curve falls monotonically. The same holds for the lower intensities used in Figs. 1 and 3. This continuous descent of the threshold is not found in the exact solution, because instead of a mean-field charge distribution at the core the two electrons are treated as quantized charges. So either two electrons or one are at the core and a continuous transition

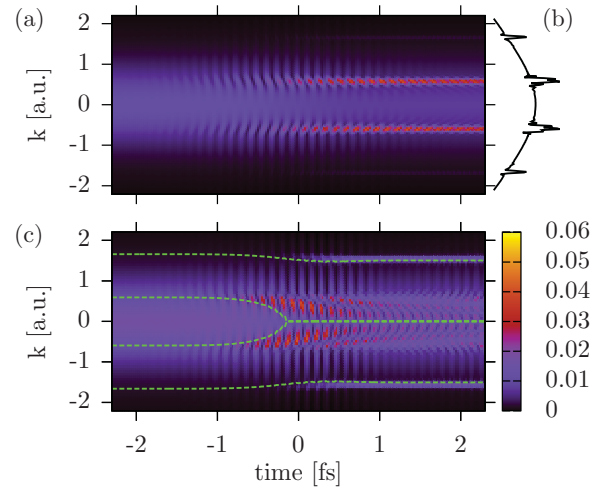


FIG. 4. (Color online) Time evolution of the electron probability density in k space for an excitation with intensity $I_1 = 3.5 \times 10^{14}$ W/cm² at a photon energy of $\hbar\omega = 33$ eV: (a) and (b) for the exact solution and (c) for the Hartree Fock approach. (b) displays the result for a time $t = 4.9t_p$ after the pulse maximum on a logarithmic scale. The dashed lines in (c) indicate the k values corresponding to the single-particle excess energies calculated using the time-dependent energies from Fig. 3.

between the first and the second ionization thresholds does not take place. This interpretation is supported by looking at the time evolution of the k -space distributions shown in Fig. 4. The exact solution [Fig. 4(a)] is strongly peaked at two k values of approximately ± 0.6 atomic units, corresponding to a kinetic energy $\frac{\hbar^2 k^2}{2m}$ of the released electron of 5 eV. These peaks result from the single-photon ionization starting from the fully occupied ground state. Ionization processes starting from the singly ionized state with one electron at the core are not seen on this scale because the photon energy is below the corresponding threshold. Figure 4(b) displays the k distribution taken at $t = 4.9t_p$ after the pulse maximum on a logarithmic scale. The figure reveals two additional weak peaks at $\sim \pm 1.7$ atomic units, reflecting the ionization where one electron is released after absorbing two photons. In contrast, the k -space distribution resulting from the Hartree-Fock calculation [Fig. 4(c)] shows that with progressing time electrons are released with decreasing momenta, reflecting the decreasing excess energies (dashed lines) that correspond to the rising binding energies shown in Fig. 3. As in the exact calculation the Hartree-Fock theory also predicts weaker peaks at higher momenta that are caused by two-photon single-electron processes. It has to be expected that the differences between the Hartree-Fock approximation and the exact theory are most pronounced in the two-electron system considered here. This is because, first, for larger electron numbers a mean field can build up more effectively as the contribution of a single given electron is less important, as in the two-electron case, and, second, because the difference between the ionization thresholds for single-photon ionization starting either from the ground state or from the singly ionized ion are largest in our case.

IV. MOMENTUM DISTRIBUTION FOR DOUBLE IONIZATION

In order to get more insight into the role of different ionization processes, it is worthwhile to analyze the momentum distribution of the emitted electrons, as different processes can be discriminated by corresponding characteristic k -space patterns. Such distributions can be accessed by kinetically

complete experiments that have recently been performed for neon under the excitation conditions for observing sequential double ionization using a reaction microscope [41]. Here, we shall concentrate on double-ionization processes. The double-ionization probability can be extracted by transforming the wave function into real space, where parts corresponding to neutral, singly, and doubly ionized helium can be identified according to

$$\Psi^{\text{He}}(x_1, x_2) = \begin{cases} \Psi(x_1, x_2) & \text{for } |x_1| < a, |x_2| < a, \\ 0 & \text{else,} \end{cases} \quad (4a)$$

$$\Psi^{\text{He}^+}(x_1, x_2) = \begin{cases} \Psi(x_1, x_2) & \text{for } |x_1| < a, |x_2| > a \text{ or } |x_1| > a, |x_2| < a, \\ 0 & \text{else,} \end{cases} \quad (4b)$$

$$\Psi^{\text{He}^{2+}}(x_1, x_2) = \begin{cases} \Psi(x_1, x_2) & \text{for } |x_1| > a, |x_2| > a, \\ 0 & \text{else,} \end{cases} \quad (4c)$$

where an electron is considered free when it is found at a distance larger than the threshold a from the core. Here, we chose $a = 5$ a.u. By transforming $\Psi^{\text{He}^{2+}}(x_1, x_2)$ back to the k space the momentum distribution $|\Psi^{\text{He}^{2+}}(k_1, k_2)|^2$ of two electrons emitted from the core is found.

All double-ionization processes have to fulfill energy conservation. This implies for a helium atom in the ground state with energy E_0 which absorbs n photons and ejects two electrons with the kinetic energies $E_{\text{kin}}^{(1)}$ and $E_{\text{kin}}^{(2)}$ the relation

$$E_{\text{kin}}^{(1)} + E_{\text{kin}}^{(2)} = E_0 - n\hbar\omega \quad (5a)$$

$$\Rightarrow \frac{\hbar^2 k_1^2}{2m} + \frac{\hbar^2 k_2^2}{2m} = E_0 - n\hbar\omega. \quad (5b)$$

Hence the electrons that take part in a double-ionization process are distributed on circles in k space. This is seen in Fig. 5 where we have plotted the distribution $|\Psi^{\text{He}^{2+}}(k_1, k_2)|^2$ over the corresponding momenta k_1 and k_2 for three representative photon energies at a time when the pulse is essentially gone ($4.9t_p$ after the pulse maximum). Our results at long times are in qualitatively good agreement with previous calculations of the energy distribution of the two released electrons that were performed using a 3D model [6–8,42].

With a photon energy of 60 eV [Fig. 5(a)] it is possible to remove both electrons by sequential single-photon absorptions. For sequential double ionization the allowed values for k_1 and k_2 are fully determined by the first and second ionization potentials due to energy conservation. Consequently, the characteristic trace of a sequential ionization process is a momentum distribution that is sharply peaked at discrete points on a circle [6,42]. It is clearly seen from Fig. 5 that this process indeed dominates the double ionization at 60 eV, as expected.

The photon energy of 52 eV [Fig. 5(b)] is just below the second ionization threshold at $I_p^{(2)} = 54$ eV, and thus the sequential two-photon double ionization is suppressed. The main process contributing to the double ionization in this case is the nonsequential two-photon double ionization, where both electrons are released together from the core, absorbing the energy of two photons. This process is known to lead to a continuous distribution of the momenta over the corresponding circle [6]. In contrast to the sequential ionization, the electrons here leave the core region preferentially in opposite directions, due to their mutual Coulomb repulsion that acts during their common escape. Also typical is the tendency that it is most likely that one electron gets nearly all the energy while the other escapes with rather low velocity [43]. All these characteristic features are seen in Fig. 5(b), confirming the

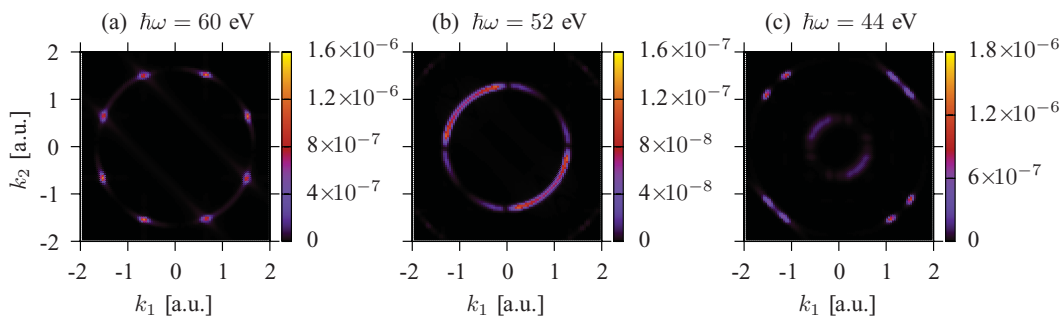


FIG. 5. (Color online) Absolute square of the two-electron wave function restricted to doubly ionized helium $|\Psi^{\text{He}^{2+}}(k_1, k_2)|^2$ at a time $t = 4.9t_p$ after the pulse maximum for an excitation intensity of $I_1 = 3.5 \times 10^{14}$ W/cm² and photon energies (a) 60 eV, (b) 52 eV, and (c) 44 eV.

expectation that by tuning the photon energy it is possible to switch between sequential and nonsequential ionization processes.

Interestingly, on lowering the photon energy further to 44 eV, we find a coexistence between sequential and nonsequential processes as seen in Fig. 5(c) by looking at the characteristic k distributions. The inner ring corresponds to nonsequential two-photon absorption while the outer ring reflects the sequential three-photon double-ionization process where first a single photon removes one electron and then the remaining electron is ripped off the core by a two-photon absorption. Looking closely at the outer ring in Fig. 5(c) it is striking that the peaks of electrons emitted in opposite directions (quadrants 2 and 4 in the figure) are much sharper than those corresponding to an emission in the same direction (quadrants 1 and 3 in the figure), which are noticeably smeared out around the circle. This is caused by the stronger influence of the Coulomb interaction when electrons fly side by side with similar velocities as compared to a situation where they fly apart and are thus largely separated. It is clear that a coexistence of two rings as seen in Fig. 5(c) can be observed only at high enough intensities. For low intensities the two-photon process always dominates over the three-photon process and thus only the inner ring is seen. To make this argument more quantitative, we have integrated the distribution $|\Psi^{\text{He}^{2+}}(k_1, k_2)|^2$ separately over the inner and outer rings in Fig. 5(c) in order to get a measure for the strengths of the corresponding processes. The results are presented in Fig. 6. As expected, at low intensities the signal rises with the square of the intensity for the two-photon process while for the three-photon process the dependence is cubic. For intensities above $\sim 10^{15}$ W/cm² both signals start to saturate even though the double-ionization probability is still below 10%. At high enough intensities the single ionization even after a short, femtosecond, pulse is almost complete and leads

to the saturation of the double-ionization signals seen in the figure.

Experimentally, the intensity scaling of ionization yields is often used to identify different pathways of the ionization process. For example, in Ref. [44] a measured scaling $\sim I^2$ of the double-ionization yield of helium has been taken as evidence for a dominance of direct two-photon ionization in this experiment. The scaling in this example coincides with the prediction obtained from lowest-order perturbation theory. At elevated intensities the situation is more complex [45], as can also be seen, e.g., from recent experiments with neon, where the intensity dependence of the total double-ionization yield has been analyzed [46]. At low intensities a quadratic scaling has been found, while at elevated intensities the exponent is between 2 and 3. This finding has been taken as an indication for a mixture between direct two-photon and sequential three-photon double-ionization processes occurring at elevated intensities.

In the following we shall discuss the intensity dependence of the total double-ionization yield that results from our 1D helium model (green crosses in Fig. 6). In order to make closer contact with experimentally accessible quantities, we have performed an average over the spatial laser profile (volume averaging), assuming a Gaussian profile with a full width at half maximum of 15 μm (black solid line in Fig. 6), which is an assumption typical for current experiments [47]. Assuming that the total volume-averaged double-ionization probability follows a power law of the form I^n , the slope in a logarithmic plot should give the exponent n . This slope is plotted in the inset of Fig. 6. As is clearly seen, the exponent first changes continuously from 2 to 2.6 until at higher intensities it drops even below 2. Obviously, for intensities above $\sim 5 \times 10^{14}$ W/cm², an exponent between 2 and 3 does not indicate a competition between two- and three-photon processes of roughly equal strength. Instead, the three-photon process clearly dominates even though the total yield does not show a cubic intensity scaling due to the saturation of the signal.

V. TIME DEPENDENCE OF THE DOUBLE IONIZATION

Advancing the available radiation sources to ever shorter pulse durations makes the temporal evolution of ionization processes a new focus of interest. First xuv-pump xuv-probe experiments [13] analyzing the fragmentation dynamics of N₂ may pave the way toward fully time-resolved measurements of ultrafast ionization processes. For excitations with short-pulse excitations, it is expected theoretically that on short times during or shortly after the pulse the dynamics should evolve coherently through coherent superposition states. This is in contrast to a time evolution described by incoherent transition rates. If the rates are not introduced phenomenologically, they are usually calculated using a golden-rule-type formula which involves a strict energy conservation between initial and final states. However, it is clear from standard textbook derivations of the golden rule that the energy-conserving δ function builds up in time. On short time scales deviations from this behavior should occur due to the energy-time uncertainty, which allows transitions in a wider energy range. Indeed, signatures of energy-time uncertainty that result from femtosecond laser excitations of semiconductors have recently been theoretically

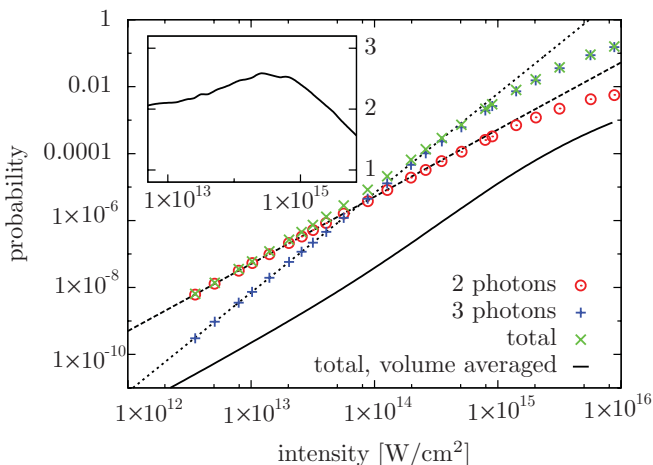


FIG. 6. (Color online) Dependence of the two- and three-photon contributions and the total double ionization probability (with and without volume averaging) on the intensity I for a photon energy of $\hbar\omega = 44$ eV [cf. Fig. 5(c)] together with fits of the form I^n to the two- and three-photon curves in the region $I < 10^{14}$ W/cm². The fit gives $n = 2$ and $n = 3$ for the two- and three-photon contributions respectively. The inset shows the slope of the volume averaged total double ionization curve.

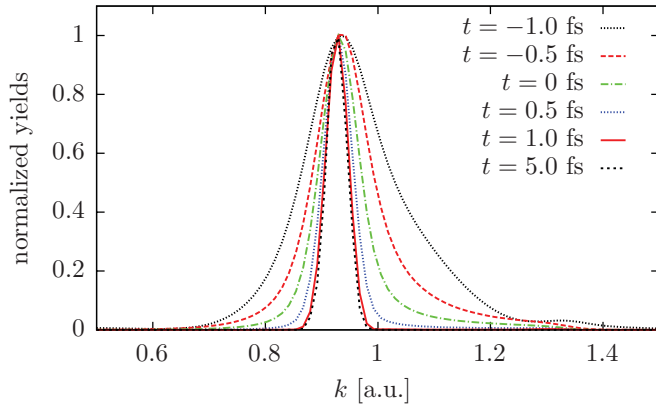


FIG. 7. (Color online) Momentum distribution of electrons emitted in opposite directions $|\Psi^{\text{He}^{2+}}(k, -k)|^2$ with equal kinetic energies for different times specified in the figure.

predicted and later measured [48]. Typically, as a result of the energy-time uncertainty, carrier distributions generated in the conduction band of a semiconductor by short laser pulses are found to be much broader directly after or during the pulse than at longer times. To quantify such effects for our system, we have plotted in Fig. 7 the momentum distribution $|\Psi^{\text{He}^{2+}}(k_1, k_2)|^2$ for different times for a photon energy of 52 eV along the line $k = k_1 = -k_2$, i.e., for the preferred emission of electrons with opposite momenta. From Fig. 5(b) we see that along the line $k = k_1 = -k_2$ two peaks occur that are symmetric around $k = 0$. In Fig. 7 we concentrate on the peak for positive k values. The curves have been normalized to their respective maxima in order to facilitate the comparison. As seen from the figure, at early times while the pulse is starting to rise, the width of the k distribution is more than twice the value found for times when the pulse has vanished. This is the characteristic signature of energy-time uncertainty. At long times the width approaches a finite value which is determined by the finite spectral width of the incoming radiation. Interestingly, the distribution in Fig. 7 is strongly asymmetric at early times, with more weight at higher k values. This may be explained by recalling that the threshold for single-electron ionization affects the double-ionization probability because singly ionized states appear as virtual intermediate states. This should provide a double-resonance structure near $k = k_1 = -k_2 = 1.3$ a.u. With strictly energy-conserving processes this resonance cannot be reached for our excitation conditions. At short times, however, the energy-time uncertainty allows some excitations close to this threshold. The usual resonant enhancement near the threshold of these excitation tails explains the enhanced distribution at higher k values in Fig. 7.

In order to learn more about the interplay of different ionization processes, it is desirable to follow their time evolution separately. To this end we recall that different processes yield characteristic traces in the k -space distribution. For example, two- and three-photon processes can be separated because they result in momenta distributed over rings with different radii (cf. Fig. 5). We can further distinguish processes where electrons are emitted in the same or in opposite directions by looking at the momentum distribution restricted to either the

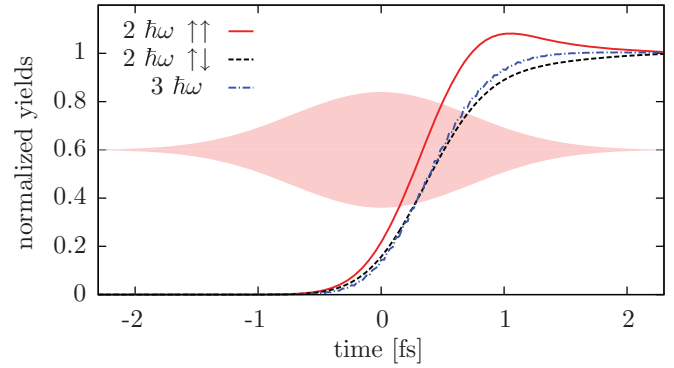


FIG. 8. (Color online) Time evolution of different contributions to the double ionization: two-photon process with electrons emitted in the same ($2\hbar\omega \uparrow\uparrow$) or in opposite ($2\hbar\omega \uparrow\downarrow$) directions and the three-photon double ionization ($3\hbar\omega$) for an excitation with intensity $I_1 = 3.5 \times 10^{14}$ W/cm² and photon energy $\hbar\omega = 52$ eV. The signals are normalized to their long-time values. The red filled area represents the envelope of the electrical field \mathcal{E} .

first and third or to the second and fourth quadrants in the k_1 - k_2 plane. Note that sequential processes emit electrons with equal probability in the same as in opposite directions [cf., e.g., Fig. 5(a)], while in a direct process the electrons are emitted preferentially in opposite directions [cf., e.g., Fig. 5(b)].

By integrating over the respective areas in the k_1 - k_2 plane, we can obtain a measure for the corresponding processes. These integrated quantities are shown in Fig. 8 as functions of time for an excitation intensity of 3.5×10^{14} W/cm² and a photon energy $\hbar\omega = 52$ eV. For better comparison all curves have been scaled to their long-time values. In contrast to the decrease of the ground-state occupation (cf. Fig. 2), the rise of all contributions in Fig. 8 sets in essentially only after the pulse has reached its maximum. This delay reflects the time taken by electrons to travel a sufficient distance from the core to be counted as emitted [cf. Eq. (4c)]. The amplitudes of two-photon emission in the opposite direction and three-photon double ionizations rise monotonically on essentially the same time scale. In contrast, emissions of two electrons in the same direction start slightly earlier and exhibit a nonmonotonic time dependence. A possible explanation for this nonmonotonic behavior is the fact that electrons emitted in the same direction repel each other, and thus there is a certain probability that one of the electrons returns to the core area after it has first left this region. In a previous study for excitations far below the second ionization threshold, the almost complete suppression of two-electron emission in the same direction, which is typically found at long times for these excitation conditions, has been attributed to this recapture process [9]. Our results in Fig. 8 indicate that recapture processes are still noticeable but much weaker in the regime slightly below the second ionization threshold studied here.

VI. CONCLUSIONS

We have studied the near- K -shell ionization dynamics in the presence of an ultrashort intense vuv pulse. Concentrating on a 1D helium model allows us to identify signatures of

correlated electron dynamics by comparing time-dependent Hartree-Fock calculations with the full numerical solution of the corresponding Schrödinger equation. For not too high intensities the Hartree-Fock approximation reproduces well the numerically complete solution for the dynamics of the ground state, which reflects the progress of the ionization and is dominated by the single-ionization process. Both the full and approximate solutions also predict for resonant excitation of the K edge a strong depopulation of the ground state during the pulse. This indicates a massive change of the electronic structure already before the pulse reaches its maximum, which should also affect diffracted signals that are generated on the same time scale. However, the Hartree-Fock theory predicts a continuous flow of charge away from the core that is accompanied by a gradual increase of the binding of the remaining charges. This picture is not supported by the full theory, where the ionization process is quantized and the transition between electrons experiencing the first or the second ionization potential is abrupt. The Hartree-Fock approach strongly deviates from the Schrödinger theory even with respect to quantities dominated by single-ionization processes whenever the intensity is so high that the time-dependent Hartree-Fock binding energy of the remaining electron falls below the single-photon energy.

We have analyzed the momentum distribution of the electrons emitted in a double-ionization process. In qualitative agreement with 3D calculations, we find sequential two-photon double ionization for excitations above the second ionization potential and nonsequential double ionization close below this threshold. With further lowering of the photon energy for the same intensity a competition between non-sequential two-photon and sequential three-photon double

ionization occurs. It turns out that only for low intensities do the respective signals for two- and three-photon processes scale quadratically or cubically with intensity, while at higher intensities saturation effects take place even though the total double-ionization probability is lower than 10%. On increasing the intensity beyond the point where both processes have equal weight, the three-photon process clearly dominates although the total signal follows a power law with an exponent that can be far below 3. An analysis of the time evolution of the two-electron momentum distribution reveals that at short times during the excitation the distribution is asymmetric and more than twice the width at long times. The broadening reflects the influence of the energy-time uncertainty, which is a strong indication for a coherent regime that occurs in the dynamics for sufficiently short excitations. The asymmetry may be attributed to the vicinity to a virtual resonance. Separation of the time evolution of different double-ionization processes reveals that the two-photon process with the emission of both electrons in opposite directions shows practically the same time dependence as the three-photon process. In contrast, the two-photon double ionization where the electrons are emitted in the same direction is affected by recapture processes that lead to a nonmonotonic time dependence of the corresponding yield.

ACKNOWLEDGMENTS

We gratefully acknowledge the financial support by the Bundesministerium für Bildung und Forschung BMBF through Grants No. 05K10WCA and No. 05K10PSB. We also acknowledge stimulating discussions with I. D. Feranchuk and D. Hochstuhl.

-
- [1] H. N. Chapman *et al.*, *Nature Phys.* **2**, 839 (2006).
 - [2] B. W. J. McNeil and N. R. Thompson, *Nat. Photonics* **4**, 814 (2010).
 - [3] R. Neutze, R. Wouts, D. van der Spoel, E. Weckert, and J. Hajdu, *Nature (London)* **406**, 752 (2000).
 - [4] S. P. Hau-Riege, R. A. London, H. N. Chapman, and M. Bergh, *Phys. Rev. E* **76**, 046403 (2007).
 - [5] S. P. Hau-Riege, *Phys. Rev. A* **76**, 042511 (2007).
 - [6] X. Guan, K. Bartschat, and B. I. Schneider, *Phys. Rev. A* **77**, 043421 (2008).
 - [7] J. Feist, S. Nagele, R. Pazourek, E. Persson, B. I. Schneider, L. A. Collins, and J. Burgdörfer, *Phys. Rev. A* **77**, 043420 (2008).
 - [8] A. Palacios, T. N. Rescigno, and C. W. McCurdy, *Phys. Rev. A* **79**, 033402 (2009).
 - [9] E. Fomouou, A. Hamido, P. Antoine, B. Piraux, H. Bachau, and R. Shakeshaft, *J. Phys. B* **43**, 091001 (2010).
 - [10] J. S. Parker, L. R. Moore, K. J. Meharg, D. Dundas, and K. T. Taylor, *J. Phys. B* **34**, L69 (2001).
 - [11] I. A. Ivanov and A. S. Kheifets, *Phys. Rev. A* **75**, 033411 (2007).
 - [12] R. Shakeshaft, *Phys. Rev. A* **76**, 063405 (2007).
 - [13] A. Rudenko *et al.*, *J. Phys. B* **43**, 194004 (2010).
 - [14] S. Fritzsche, A. N. Grum-Grzhimailo, E. V. Gryzlova, and N. M. Kabachnik, *J. Phys. B* **41**, 165601 (2008).
 - [15] A. S. Kheifets, *J. Phys. B* **42**, 134016 (2009).
 - [16] M. Richter, M. Y. Amusia, S. V. Bobashev, T. Feigl, P. N. Juranic, M. Martins, A. A. Sorokin, and K. Tiedtke, *Phys. Rev. Lett.* **102**, 163002 (2009).
 - [17] N. Rohringer and R. Santra, *Phys. Rev. A* **76**, 033416 (2007).
 - [18] M. G. Makris, P. Lambropoulos, and A. Mihelic, *Phys. Rev. Lett.* **102**, 033002 (2009).
 - [19] K. Balzer, S. Bauch, and M. Bonitz, *Phys. Rev. A* **82**, 033427 (2010).
 - [20] K. C. Kulander, *Phys. Rev. A* **36**, 2726 (1987).
 - [21] D. Hochstuhl and M. Bonitz, *J. Chem. Phys.* **134**, 084106 (2011).
 - [22] J. Caillat, J. Zanghellini, M. Kitzler, O. Koch, W. Kreuzer, and A. Scrinzi, *Phys. Rev. A* **71**, 012712 (2005).
 - [23] J. J. Carrera and Shih-I. Chu, *Phys. Rev. A* **79**, 063410 (2009).
 - [24] Y. Ding *et al.*, *Phys. Rev. Lett.* **102**, 254801 (2009).
 - [25] B. Nagler *et al.*, *Nature Physics* **5**, 693 (2009).
 - [26] A. A. Sorokin, S. V. Bobashev, T. Feigl, K. Tiedtke, H. Wabnitz, and M. Richter, *Phys. Rev. Lett.* **99**, 213002 (2007).
 - [27] M. Richter, S. V. Bobashev, A. A. Sorokin, and K. Tiedtke, *J. Phys. B* **43**, 194005 (2010).
 - [28] J. Feist, S. Nagele, R. Pazourek, E. Persson, B. I. Schneider, L. A. Collins, and J. Burgdörfer, *Phys. Rev. Lett.* **103**, 063002 (2009).

- [29] B. Piraux, J. Bauer, S. Laulan, and H. Bachau, *Eur. Phys. J. D* **26**, 7 (2003).
- [30] M. Meyer *et al.*, *Phys. Rev. Lett.* **104**, 213001 (2010).
- [31] L. Young *et al.*, *Nature* **466**, 56 (2010).
- [32] D. G. Lappas and R. van Leeuwen, *J. Phys. B* **31**, L249 (1998).
- [33] M. Lein, E. K. U. Gross, and V. Engel, *Phys. Rev. Lett.* **85**, 4707 (2000).
- [34] R. Grobe and J. H. Eberly, *Phys. Rev. Lett.* **68**, 2905 (1992).
- [35] Q. Su and J. H. Eberly, *Phys. Rev. A* **44**, 5997 (1991).
- [36] P. Emma *et al.*, *Nature Photonics* **4**, 641 (2010).
- [37] W. Ackermann *et al.*, *Nature Photonics* **1**, 336 (2007).
- [38] M. S. Pindzola, D. C. Griffin, and C. Bottcher, *Phys. Rev. Lett.* **66**, 2305 (1991).
- [39] P. Maragakis and P. Lambropoulos, *Laser Physics* **7**, 679 (1997).
- [40] N. E. Dahlen and R. van Leeuwen, *Phys. Rev. A* **64**, 023405 (2001).
- [41] M. Kurka *et al.*, *New J. Phys.* **12**, 073035 (2010).
- [42] K. L. Ishikawa and K. Midorikawa, *Phys. Rev. A* **72**, 013407 (2005).
- [43] D. A. Horner, C. W. McCurdy, and T. N. Rescigno, *Phys. Rev. A* **78**, 043416 (2008).
- [44] Y. Nabekawa, H. Hasegawa, E. J. Takahashi, and K. Midorikawa, *Phys. Rev. Lett.* **94**, 043001 (2005).
- [45] L. A. A. Nikolopoulos and P. Lambropoulos, *Phys. Rev. Lett.* **97**, 169301 (2006).
- [46] R. Moshhammer *et al.*, *Phys. Rev. Lett.* **98**, 203001 (2007).
- [47] A. A. Sorokin *et al.*, *Appl. Phys. Lett.* **89**, 221114 (2006).
- [48] V. M. Axt and T. Kuhn, *Rep. Prog. Phys.* **67**, 433 (2004).